Simulating Miniaturized Open Photoacoustic Gas Sensors

Simon Essing, Chair of Physics of Electrotechnology, Technical University of Munich, Germany, simon.essing@tum.de
Gabriele Schrag, Chair of Physics of Electrotechnology, Technical University of Munich, Germany, schrag@tum.de
David Tumpold, Infineon Technologies AG, Neubiberg, Germany, david.tumpold@infineon.com

Abstract

We demonstrate a novel approach for the simulation of miniaturized non-resonant photoacoustic gas spectroscopy (PAS) sensors by applying a one-dimensional signal flow model. Using the described method, these non-resonant PAS sensors systems can be optimized with regard to their applicability to different target gases. The model is validated with lab measurements and reveals potentials and limitations with a view to optimization endeavours.

1 Introduction

The ever-increasing need for continuous and real-time monitoring of air quality—for example that of the human-emitted pollutant carbon dioxide (CO_2)—necessitate the development of compact and energy-saving air sensor technology. Emerging non-resonant miniaturized open PAS systems provide a cheap and robust sensing mechanism, while having dimensions of just around one cubic centimetre. This enables a variety of IOT applications in the field of climate monitoring [1]. The following paper shows an approach to model a PAS system efficiently.

2 System and Model Description

Non-resonant PAS systems comprise an acoustically sealed measuring chamber containing an infrared source, an optical filter, a gas chamber containing the target gas to be sensed, and a microphone in order to measure the induced pressure variations [2].
The infrared source periodically emits optical power in a broad spectral range. A Bragg filter limits the range of the radiation entering the measuring chamber to exact the wavelength where the gas molecules to be detected absorb light, hence are sensitive to. Through absorption, these molecules are excited to elevated energy levels and generate thermal energy through collision processes with surrounding molecules when relaxing again to their ground state.
In the closed measuring chamber, this periodic heat generation causes a periodic pressure signal according to the ideal gas equation, which can be measured by using a capacitive microphone.
The higher the acoustic power detected by the microphone, the higher is the concentration of the gas absorbing at the respective wavelength inside the measuring chamber. [3]
The overall system model of the PAS consists of sub-models in the specific domains (**Figure 1**), connected to each other: The optical power of the infrared source is simulated with a detailed Finite Element Model (FEM); the transmissivity of the optical filters is modelled by applying the Transfer-Matrix Method in OpenFilters. The Absorption behavior of the target gas is calculated with the help of Python, using the absorption lines exported from the HITRAN database as a basis, considering spectral distortions due to concentration, temperature, pressure and humidity variations. Using finally Beer-Lambert's law and taking into account the optical path of the set-up, the optical power distribution inside the measurement volume is obtained.

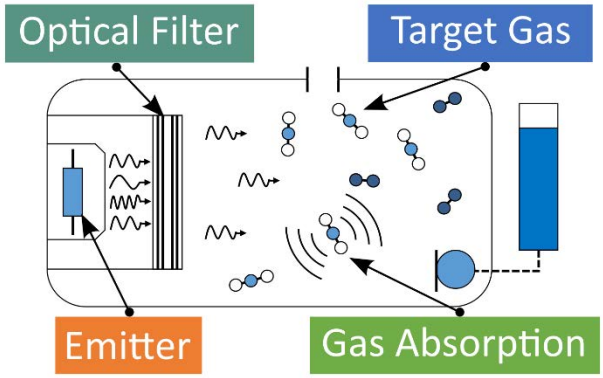

Figure 1: Signal path and subsystems to be modelled for miniaturized open PAS systems: from infrared optical power input to acoustical microphone signal.

The respective submodels necessary for simulating the measurement path of the PAS and, hence, for evaluating and optimizing its specifications for sensing a given gas species (i.e., sensitivity, selectivity) are described in the following subsections.

3 Submodel of Infrared Source

To generate radiation with wavelengths lying in the infrared band of interest, i.e., the absorption band of the gas to be sensed, a silicon MEMS heater is applied due to its miniaturized compact design and low processing cost. Recently, a lot of research has been conducted in the field of micro heaters for environmental gas sensing applications [4–6]. To simulate the optical power the silicon MEMS heater is emitting, an FEM analysis is conducted, to evaluate temperature distribution at the heater's surface in dependence of the applied bias voltage. This temperature distribution is the input to a blackbody radiation model applied to provide the resulting optical power spectrum radiating from the heaters surface into the system.

ISBN 978-3-8007-5835-7

The specific spectral intensity i_λ emitted from an ideal blackbody can be calculated applying Planck's law of radiation [7]:

$$i_\lambda = \frac{2\pi c^2 h}{\lambda^5 \left(e^{\frac{ch}{k\lambda T}} - 1\right)}$$

with the constants c being the speed of light, h being the Planck constant and k the Boltzmann constant. Integrating i_λ as a function of the temperature distribution $T(A)$ along the heater's surface assuming constant emissivity ε yields the optical power spectrum of the radiation emitted by the heater, which is shown in **Figure 2**.

$$P_\lambda = \varepsilon \int i_\lambda(T(A))\, da$$

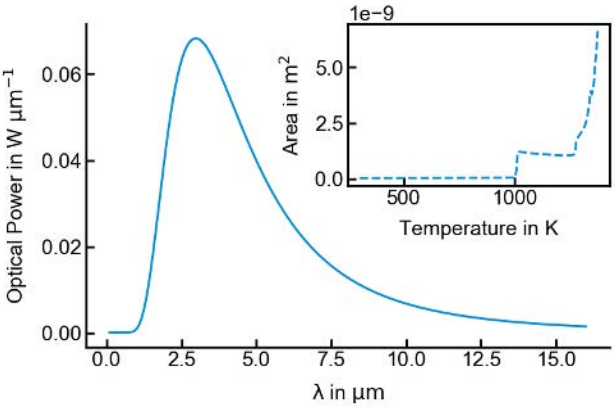

Figure 2: Simulated emitted optical power of a MEMS infrared heater. The temperature distribution at the heater's surface serves as input for the model of the ideal blackbody radiation, assuming constant emissivity $\varepsilon = 1$.

4 Submodel of the Filter

To suppress optical power of unwanted wavelengths, a Bragg filter is modelled, transmitting only in the range of CO_2 absorptivity. The filter is designed with the open source software OpenFilters. [8]

Modelling the transmission of a filter consisting of alternating and ideal Si and SiO_2 layers is most effectively done using the transfer matrix method which is described in detail in [9]. To get an optical bandpass filter optimized for CO_2, two stacks of layers need to be deposited on either side of a silicon substrate, each representing a damping band. Tuning the filter thicknesses of each layer in the stack, an optimized transmission band is obtained, see **Figure 3**.

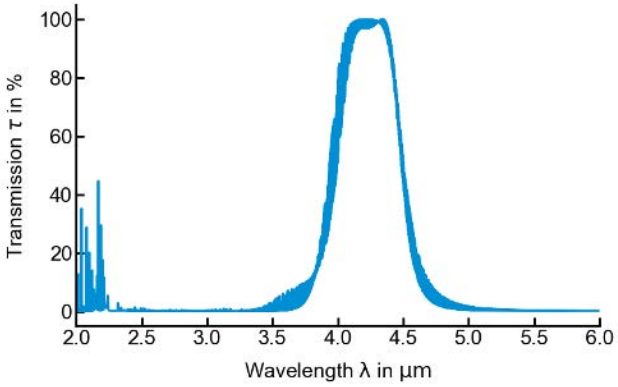

Figure 3: Simulated transmission of a Si-SiO_2 filter stack, suppressing transmission of optical Power on both sides of the absorption spectra of CO_2.

5 Modelling the Absorption by the Target Gas

The optical absorption capability is determined by the absorption cross-section of the gas molecule. If optical radiation of a certain wavelength is absorbed by a molecule, it enters an excited state in the form of a corresponding oscillation. The absorption cross section σ_λ of a gas indicates the probability that a photon having the corresponding energy is absorbed. It depends on the molecular configuration of the absorbing gas, the energy content of the exciting photon and the distortion of the absorption line by temperature and pressure. For CO_2 under normal conditions the absorption cross section σ_λ for wavelengths between 1 µm and 16 µm is calculated and displayed in **Figure 4.**

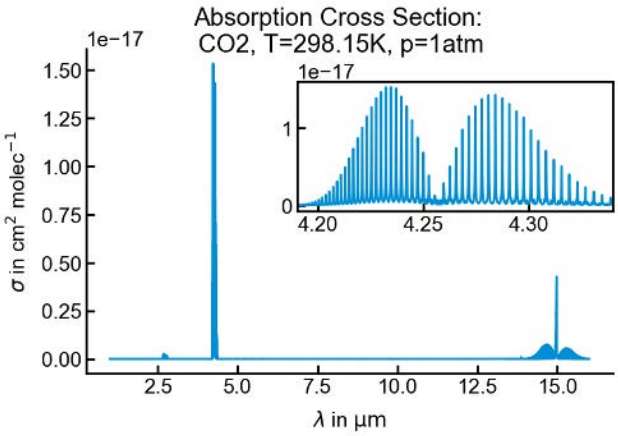

Figure 4: Absorption cross section of CO_2 under normal conditions. The highest absorption probability is between 4.2 µm and 4.4 µm where CO_2 shows its characteristic comb like absorption structure.

To calculate the absorption spectra of the gas atmosphere inside the photoacoustic sensor as a function of the concentration q, pressure p and temperature T, the Beer-Lambert's law is applied:

$$\alpha_\lambda = 1 - e^{-\frac{qpx}{kT}\sigma_\lambda}$$

Here, x denotes the optical path inside the photoacoustic chamber, which depends on the geometrical and reflective properties of the photoacoustic system.

6 Calculation of the Generated Pressure Variations

The pressure variation $P(t)$ inside the measurement chamber depends on the change in the number of excited molecules N_1. In the following, the respective calculation steps are sketched, a more detailed deduction can be found in [10].
The change of the excited molecules N_1 contained in the system satisfies the following differential equation:

$$\frac{dN_1}{dt} + \frac{N_1}{\tau_e} = A_{01}N_0$$

Here, N_0 denotes the number of unexcited particles, A_{01} stands for the average excitation time of a molecule from the unexcited state "0" to the excited state "1", and τ_e describes the average lifetime of an excited state. This equation can be solved for harmonic excitations and assuming that the total particle number N is approximately equal to that of the unexcited particles N_0:

$$N_1(t) = \frac{1}{2}N\tau_e A_{01}\left(\frac{M\sin(\omega t - \tan^{-1}(\omega\tau_e))}{\sqrt{1+\omega^2\tau_e^2}} + 1\right)$$

Here, the factor M is used for the modulation depth of the light source. The change of the molecular kinetic energy within an isochoric gas volume requires a pressure variation—for a photoacoustic system, however, this is only possible via the non-radiative relaxation discussed in the previous paragraph. The dissipation of this thermal energy must take place via the chamber wall and can be expressed via the time constant τ_{th}. For the time-dependent pressure signal, this results in the following relationship:

$$P(t) = \frac{(\gamma-1)\tau_e\tau_{th}}{2\tau_{VT}}\zeta N A_{01} \times \left(\frac{M\sin(\omega t - \tan^{-1}(\omega\tau_e) - \tan^{-1}(\omega\tau_{th}))}{\sqrt{1+\omega^2\tau_e^2}\sqrt{1+\omega^2\tau_{th}^2}} + 1\right)$$

Here, γ denotes the isentropic exponent, which is the ratio of the isobaric and isochoric heat capacities of a gas: $\gamma = C_p/C_v$. The average time constant for a molecular non-radiative relaxation is τ_{VT}. The parameter ζ indicates the excitation energy of a single excited state—the relation between excitation energy and the wavenumber ν of an exciting photon requires the speed of light c as well as Planck's constant h and reads as: $\zeta = hc\nu$. The Fourier transform of the pressure signal yields the photoacoustic pressure signal, which depends on the excitation frequency, analogous to the time-dependent pressure signal $P(t)$:

$$P(j\omega) = \frac{(\gamma-1)\zeta N A_{01} M}{\tau_{VT}(j\omega + \tau_e^{-1})(j\omega + \tau_{th}^{-1})}$$

To illustrate the implications of the relationship, an exemplary response for the photoacoustic excitation of CO_2 at a concentration of 1000 ppm when using the infrared heater and the Bragg filter in a typical detection chamber is shown in **Figure 5**. Note in particular the characteristic corner frequencies, which reflect the influence of the three different time constants τ_{VT}, τ_{th} and τ_e, respectively.

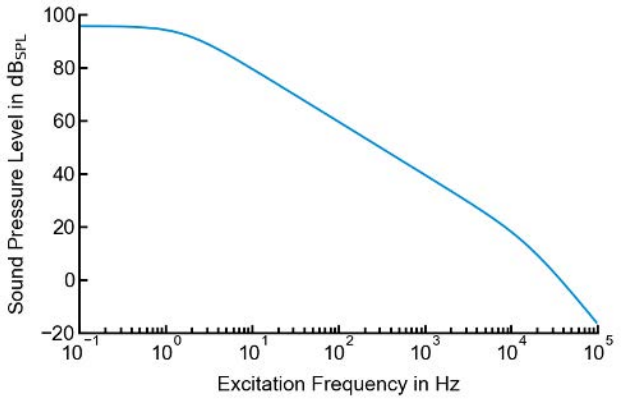

Figure 5: Sound pressure level inside the photoacoustic system depending on the excitation frequency of the light source. With increasing frequency, the photoacoustic pressure decreases.

Calculating the photoacoustic pressure inside the system applying the previous submodels, yields a frequency-dependant photoacoustic pressure signal inside the system, shown in **Figure 6**. Choosing the microphone's sensitivity at the specific excitation frequency with regard to the lowest detectable pressure signal provides the estimated limit of detection in ppm—thus giving a direct figure of merit of a potential sensor prototype.

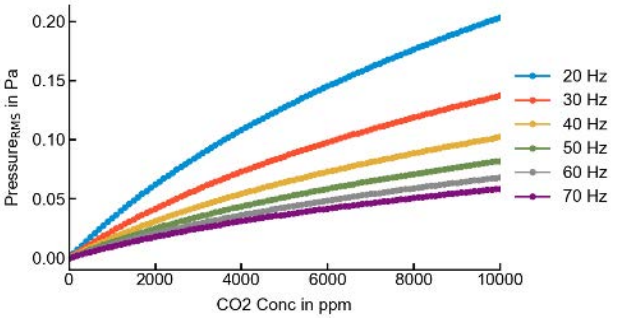

Figure 6: Simulated pressure levels inside the photoacoustic system depending on the excitation frequency of the light source and the gas concentration.

ISBN 978-3-8007-5835-7

7 Summary of Results

We presented a comprehensive simulation procedure, which enables to model the signal path in a miniaturized photoacoustic gas sensor (PAS). Applying the presented model, we are able to predict the requirements a PAS must meet in order to detect certain gases with the required accuracy. This way, the sensitivity of PAS prototypes can be estimated and tailored in advance in order to predict sensor performance by means of virtual prototyping. The model is calibrated and validated with experimental data. Optimizing subcomponents of the system by tuning the characteristics of the emitter, the filter or the detection chamber leads to a close to real world estimate of the sensor performance, paving the way to even more miniaturized future photoacoustic gas sensors.

8 Literature

[1] Infineon Technologies AG, "XENSIV™ Environmental Sensor," Neubiberg, Germany, 2020.

[2] S. Palzer, "Photoacoustic-Based Gas Sensing: A Review," *Sensors (Basel, Switzerland)*, vol. 20, no. 9, 2020, doi: 10.3390/s20092745.

[3] G. Gerlach, U. Guth, and W. Oelßner, *Carbon dioxide sensing: Fundamentals, principles, and applications*, 2019.

[4] V. Komenko, A. Kravchenko, and W.-J. Fischer, "Silicon-On-Nothing IR-Emitter for Gas Sensing Applications," *Proceedings*, vol. 2, no. 13, p. 1080, 2018, doi: 10.3390/proceedings2131080.

[5] S. Biermann *et al.,* "Advanced broadband MEMS infrared emitter based on high-temperature-resistant nanostructured surfaces and packaging solutions for harsh environments," in *Terahertz, RF, Millimeter, and Submillimeter-Wave Technology and Applications XIII*, San Francisco, United States, Feb. 2020 - Feb. 2020, p. 7. [Online]. Available: https://www.spiedigitallibrary.org/conference-proceedings-of-spie/11279/2545119/Advanced-broadband-MEMS-infrared-emitter-based-on-high-temperature-resistant/10.1117/12.2545119.full

[6] Z. E. Jeroish, K. S. Bhuvaneshwari, F. Samsuri, and V. Narayanamurthy, "Microheater: material, design, fabrication, temperature control, and applications-a role in COVID-19," *Biomedical microdevices*, vol. 24, no. 1, p. 3, 2021, doi: 10.1007/s10544-021-00595-8.

[7] P. Böckh and T. Wetzel, *Wärmeübertragung*. Berlin, Heidelberg: Springer Berlin Heidelberg, 2017.

[8] S. Larouche and L. Martinu, "OpenFilters: open-source software for the design, optimization, and synthesis of optical filters," *Applied optics*, vol. 47, no. 13, C219-C230, 2008.

[9] H. A. Macleod, *Thin-film optical filters*. Boca Raton, FL: CRC Press, Taylor & Francis Group, 2018.

[10] O. Schulz, H. Kern, H. Wurmus, and G. Müller, *Bestimmung physikalischer und technischer Randbedingungen zur Umsetzung eines photoakustischen Gassensors in der Mikrosystemtechnik*. @Ilmenau, Techn. Univ., Diss., 2007. Ilmenau: Univ.-Bibliothek; Univ.-Verl. Ilmenau, 2008. [Online]. Available: http://www.db-thueringen.de/servlets/DocumentServlet?id=10278

